Role Dynamic Assignment of Human–Robot Collaboration Based on Target Prediction and Fuzzy Inference

Chengyun Wang and Jing Zhao

***Abstract*—Aiming to solve the problem of role dynamic assignment in human–robot collaborative motion with unknown and changeable targets, a role dynamic assignment method based on target prediction and fuzzy inference is proposed. First, a human–robot collaborative motion framework based on role dynamic assignment is constructed. Then, based on the analysis of the human–robot collaborative motion with fixed role (HMFR), a human–robot collaborative motion target prediction module, a role dynamic assignment module, and a robot motion planning module are designed to realize the role dynamic assignment and motion planning of the robot. Finally, human–robot collaborative motion experiments based on role dynamic assignment are performed. Experimental results show that the proposed role dynamic assignment algorithm can effectively implement role dynamic assignments. Compared with the human–robot collaborative motion with fixed roles, the human–robot collaborative motion based on role dynamic assignment has better overall performance in terms of actual path and desired path similarity (Fréchet distance) and participant workload.**

***Index Terms*—Fuzzy inference, human–robot collaborative motion, motion planning, role dynamic assignment, target prediction.**

I. Introduction

ROBOTS are good at autonomously executing tasks on predetermined trajectories. Humans are good at reasoning and problem solving and can give robots task correction, fine-tuning control, and situational guidance. Combining these advantages in some human–robot collaborative tasks can achieve complementary advantages, such as telemanipulation [1], [2], collaborative assembly [3], [4], and collaborative transportation [5], [6].

In traditional human–robot collaborative tasks, human and robot roles are fixed. The human/robot always plays the "leader" role, and the robot/human plays the follower role. In human-leader tasks, humans are always required to lead the task and guide the robot, and the robot usually obeys human motion. This means that humans are constantly under a high cognitive load, degrading human–robot collaborative performance over time. Although in special application scenarios, such as surgical robots [7] and exoskeleton robots [8], it is suitable for humans to play the leading role all the time, this is the direct result of the nature of the task. It may not be suitable for other application scenarios, such as obstacle avoidance [9]. When the robot senses an impending collision, the robot can directly take the lead and automatically modify the human motion. In tasks led by robots, tasks can be completed by the robot with high accuracy, such as collaborative welding [10]. In the welding process, robots can conduct more accurate welding according to preplanned trajectories. However, it is not cost-effective to accurately determine the robot trajectories required for each workpiece variant in high mixing and low batch manufacturing. Therefore, it is necessary to assign the roles of humans and robots according to the task situation to realize the complementary advantages of humans and robots [11].

Robot role assignment methods are generally divided into role static and dynamic assignment methods. The role static assignment method generally divides the task into two different subtasks according to the task information. Then, it assigns different subtasks to humans and robots, and the humans and robots play the "leader" role in their respective subtasks [12]. For example, in the chainsaw task [13], the task is divided into two subtasks, "push" and "pull." When a human performs the "pull" subtask, the human is the leader, and the robot is the follower. When the human performs the "push" subtask, the robot plays the "leader" role, and the human plays the "follower" role. The role static assignment method is suitable for situations where the task can be divided into different subtasks, and each subtask conforms to the working characteristics of the human or the robot. However, the role static assignment method is not applicable when tasks cannot be divided into different subtasks or the boundaries of subtasks are fuzzy. Therefore, it is necessary to dynamically assign the human and robot roles according to task information, such as human–robot collaborative transportation tasks [14]. The beginning and stopping phases of collaborative transportation tasks are suitable for humans to play the "leader" role to cope with the changing situation. The middle phase is suitable for robots to play the "leader" role because the motion

Manuscript received 13 February 2023; accepted 1 April 2023. Date of publication 11 April 2023; date of current version 11 December 2023. This work was supported by the National Natural Science Foundation of China under Grant 51975008. Paper no. TII-23-0487. *(Corresponding author: Jing Zhao.)*

The authors are with the Faculty of Materials and Manufacturing, Beijing University of Technology, Beijing 100021, China (e-mail: 623935104@qq.com; zhaojing@bjut.edu.cn).

Color versions of one or more figures in this article are available at https://doi.org/10.1109/TII.2023.3266378.

Digital Object Identifier 10.1109/TII.2023.3266378

is stable. However, the division of the three motion phases is fuzzy, and in different motion phases, both humans and robots may become the leader. For example, the continuous increase in the human interaction force at any motion position indicates that humans have clear leader intentions, and the robot should yield and become the follower. Therefore, it is necessary to dynamically assign the roles of humans and robots according to external information and the changes in the phase of the human–robot collaborative motion.

The dynamic assignment of the human and robot roles can be realized through vision, voice, or touch combined with situational information [15]. For example, in [16], the human and robot roles were dynamically adjusted through various trigger events, such as sound, distance from the target, and human–robot interaction force. In [17], humans and robots expressed their intentions through gestures to achieve role transformation. In [18], the roles were dynamically assigned according to the symbols of interactive force, motion velocity, and acceleration of human–robot collaborative motion. In [19], [20], and [21], the methods of the interaction force threshold and energy threshold were adapted to adjust the role dynamically. When the interaction force or energy continues to increase and exceeds the set threshold, the human will become the leader. In [22], a cost function for interaction force and task performance was established to describe the collaborative behavior between humans and robots. The roles were dynamically assigned by optimizing the cost function. In [23], the task performance index based on interaction force is established, and the role is assigned by analyzing the task performance of the collaborative partner. The individual with higher task performance will assume the role of leader. In [24] and [25], a role dynamic assignment (RDA) algorithm based on the homotopy method was established. In [26], the human and robot roles were dynamically assigned based on the game theory method. In the abovementioned RDA method, the robot knows the target position and the task content to preplan its own motion trajectory, while the human only acts as the task corrector [27], [28]. Specifically, when the robot plays the "leader" role, the robot moves according to the preplanned trajectory; when the robot's motion trajectory does not meet the task requirements, the human plays the "leader" role to intervene (correct) with the robot's motion. However, in tasks with unknown and variable targets, the robot trajectory cannot be preplanned; thus, the above RDA method is no longer applicable, as shown in the human–robot collaborative assembly scenario in Fig. 1.

In the human–robot collaborative assembly, the robot is required to assemble the workpiece on conveyor belt A and the workpiece on conveyor belt B together. Due to the different shapes of the workpiece each time, the error of the placement position of the assembly workpiece, and the changing assembly sequence, the robot's motion trajectory cannot be preplanned. The workers can guide the robot to move the workpiece to the assembly position through interactive force, but the workers frequently guide the robot to repeat the motion, which consumes considerable mental and physical resources and leads to worker fatigue. In addition, due to the participation of humans, the motion path is an irregular arc, resulting in unstable motion.

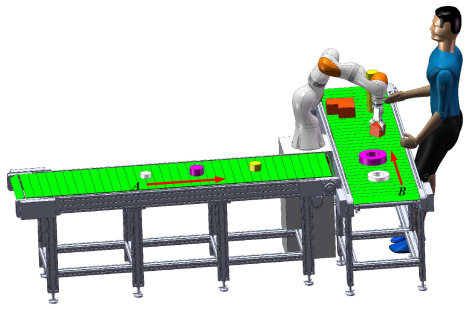

Fig. 1. Human–robot collaborative assembly scenario.

Therefore, it is necessary to reduce human participation in human–robot collaborative motion. The way to reduce human participation in human–robot collaborative motion is to assign the robot's role dynamically. Under appropriate conditions, the robot plays the "leader" role to lead the human–robot collaborative motion instead of the human leading the task progress all the time.

Based on the abovementioned analysis, this article first proposes a human–robot collaborative motion framework consisting of three modules: target prediction, role dynamic assignment, and robot motion planning. Second, based on the human–robot collaborative assembly task analysis, the experiment of the human–robot collaborative motion with fixed roles (HMFR) is designed, and the HMFR dataset is established. Aiming at the problem of unknown and variable targets in human–robot collaborative motion, a target prediction module based on the Gaussian process regression method is established in this study. The robot can predict the target of the human according to the partial trajectory of the human–robot collaborative motion. RDA of the human–robot collaborative motion is similar to RDA of the human–human collaborative motion, both of which aim at the question of when the two sides of the collaborative motion play the "leader" role. However, both sides of the collaborative motion are fuzzy about when to play the "leader" role. Therefore, based on HMFR data analysis, this study establishes an RDA strategy consisting of the quantization factor selection fuzzy controller and the role assignment fuzzy controller and designs the membership functions and the fuzzy inference rules of the fuzzy controller. Compared with the existing role assignment methods, the RDA strategy combines the predicted target position, prediction probability, motion trajectory, and interaction force to imitate the experience of human experts to assign roles. The RDA strategy enables robots to make intelligent role decisions based on motion information similar to humans, thus, reducing human participation in human–robot collaborative motion. In human–robot collaborative motion with role dynamic assignment (HMRDA), the robot not only needs to know when to switch roles but also needs to know how to plan its motion when playing different roles. Therefore, the robot motion planning module is introduced. According to the different roles of the robot, the robot motion planning module is divided into a humanlike motion planning submodule and an admittance control-based motion planning submodule. These

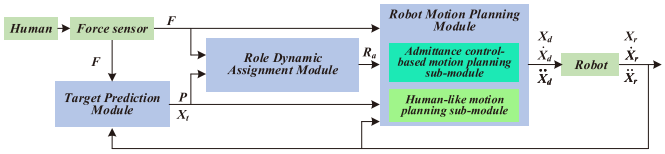

Fig. 2. HMRDA block diagram.

two submodules plan the robot's motion when it plays the "leader" and "follower" roles, respectively. Finally, the HMRDA experiment is conducted. The experimental results are compared with the HMFR experiment.

The main contributions of this work are as follows.

1) A three-module HMRDA framework is proposed to realize human–robot collaborative motion better.
2) Based on the analysis of human–robot collaborative motion, a role dynamic assignment method based on target prediction and fuzzy reasoning is proposed. According to the motion information and prediction information, the robot can adjust its role in the human–robot collaborative motion by imitating humans' logical reasoning thinking to give full play to the advantages of humans and robots.

The rest of this article is organized as follows. Section II presents a HMRDA framework. Section III presents the target prediction module. Section IV presents role dynamic assignment module. Section V presents the robot motion planning module. Section VI is HMRDA experiment. Finally, Section VII concludes this article.

II. HMRDA Framework

The HMRDA framework is composed mainly of three modules—the target prediction module, RDA module, robot motion planning module, as shown in Fig. 2. The target prediction module is a target prediction algorithm obtained by training the Gaussian process regression model with the early motion of HMFR as the dataset. In HMRDA, the robot cannot prepredict the target that the human intends to go to; thus, the robot needs the human to guide the robot to move first through interaction forces, (that is, the human plays the "leader" role). The target prediction module can predict the target that the human intends to go to and output the prediction probability based on the early motion information.

The RDA module is a robot role assignment method based on the summary of the experience of human experts in HMFRs. In the RDA module, the fuzzy inference rules of the quantization factor, the fuzzy inference rules of RDA, and the membership functions are designed through the statistical analysis of HMFR.

In HMRDA, robots not only need to know when and how to change roles but also need to plan their motions when playing corresponding roles [15]. Therefore, the robot motion planning module is introduced. The robot motion planning module is divided into admittance control-based motion planning submodules and humanlike motion planning submodules according to the different roles played by the robot in the human–robot collaborative motion. The admittance control-based motion planning submodule is mainly used for robot motion planning when the robot plays the "follower" role. When the robot plays the "follower" role, it needs human interaction force to guide its motion, and the robot is in the motion state of complying with human motion. Therefore, the admittance control method is introduced to realize the compliant motion of the robot. The humanlike motion planning submodule is mainly used for robot motion planning when the robot plays the "leader" role. When the robot plays the "leader" role, the robot is in the active motion state of guiding human–robot collaboration. To make the robot's motion more consistent with human subjective cognition and more acceptable to humans, a humanlike motion planning method is introduced. This method uses the law of human arm motion to plan the robot's motion, so the robot's motion is more in line with the subjective cognition of the human. This will improve human satisfaction with human–robot collaborative motion and the stationarity of robot motion. The following sections describe each of the three modules.

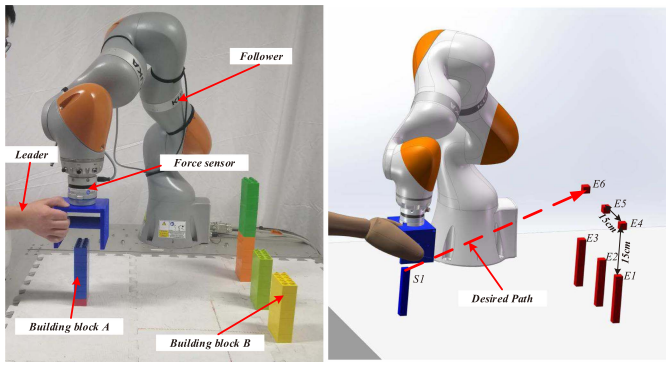

Fig. 3. Human–robot collaborative point-to-point motion experiment. Human–robot collaborative scene is shown in (a). Human–robot collaborative starting point and target setting are shown in (b).

III. Target Prediction Module

A. HMFR Experiment

As discussed in the abovementioned section, both the target prediction module and RDA module are established based on HMFR analysis. Therefore, combined with the working scene of the human–robot collaborative assembly in Fig. 1, the human–robot collaborative point-to-point motion experiment with fixed roles was designed, as shown in Fig. 3. The robot always plays the "follower" role in the HMFR experiment.

The HMFR experimental system is mainly composed of a 7-degree-of-freedom manipulator (robot LBR IIWA, KUKA, Germany) and a 6-D force sensor (HEX-E, Onrobot, Denmark) mounted on the manipulator's end effector. Participants move collaboratively with the robot using a handle attached to a force sensor. The force sensor collects the interaction force between humans and robots and transmits the collected force data to the admittance control-based motion planning submodule. The admittance control-based motion planning submodule outputs the position and other information to the robot to keep the robot

in the following state. In Fig. 3(a), blocks A and B correspond to the starting and target points of the human–robot collaborative point-to-point motion. A total of six target points (E1-E6) were set, and the distance between adjacent points was 15 cm, as shown in Fig. 3(b). The participant (leader) guides the robot (follower) by an interactive force from the starting position along the desired path [red dotted line in Fig. 3(b)] to the target point. Before the HMFR experiment, each participant performed a preexperiment to familiarize himself/herself with the experiment's content. Each target point's collaborative motion was repeated ten times. Six healthy participants (mean $age = 27 \pm 3$ years and $height = 175 \pm 6$ mm) participated in the HMFR experiment. Six participants were right-handed. A total of 360 ($6 \times 6 \times 10$) experiments were conducted, and experimental data were collected. The participants gave informed consent about their participation in the experiment. These experimental data include the robot motion path, velocity, acceleration, and interaction force.

B. Target Prediction Algorithm

To realize the role dynamic assignment and motion planning when the robot plays the "leader" role, a target prediction algorithm based on Gaussian process regression was established. Gaussian process regression is a type of machine learning regression method that has good adaptability to dealing with complex problems such as high dimensions, small samples and nonlinearity. The general regression model is

$$Y = f(\mathbf{X}) + \varepsilon \tag{1}$$

where $\mathbf{X}$ is the input vector, $f(\mathbf{X})$ is the function value, and Y is the observed value after additive noise pollution. $\varepsilon \sim N(0, \sigma_n^2)$ is the additive noise.

Equation (1) can be expressed as Gaussian process regression model [29]

$$Y \sim GP[u(\mathbf{X}), \boldsymbol{K}(\mathbf{X}, \mathbf{X}) + \sigma_n^2 \mathbf{I}_n] \tag{2}$$

where $\boldsymbol{K}(\mathbf{X}, \boldsymbol{X}) = E[(f(\boldsymbol{X}) - u(\boldsymbol{X}))(f(\boldsymbol{X}) - u(\boldsymbol{X}))^T]$, $u(\boldsymbol{X}) = E(f(\boldsymbol{X}))$, the symbol E means to find the expectation, and $\boldsymbol{K}(\boldsymbol{X}, \boldsymbol{X})$ is the covariance function (i.e., the Gaussian kernel function).

The Gaussian kernel function is

$$\boldsymbol{K}(\boldsymbol{X}_i, \boldsymbol{X}_j) = \sigma_f^2 \exp(-\|\boldsymbol{X}_i - \boldsymbol{X}_j\|^2 / 2l^2) \tag{3}$$

where σ_f is the kernel function's standard deviation, describing the input variable's local correlation, l is the characteristic length-scale, controlling the smoothness of the kernel function, and σ_f and l are called the hyperparameter.

To optimize the hyperparameters of gaussian process regression, a training dataset is established. The input datasets contain the robot end-effector's motion position $\boldsymbol{X}_r = [x_r, y_r, z_r]$, velocity $\dot{\boldsymbol{X}}_r = [\dot{x}_r, \dot{y}_r, \dot{z}_r]$, acceleration $\ddot{\boldsymbol{X}}_r = [\ddot{x}_r, \ddot{y}_r, \ddot{z}_r]$, and interaction force $\mathbf{F} = [f_x, f_y, f_z]$. The output dataset includes the data of the robot end-effector's position $\boldsymbol{X}_f = [x_f, y_f, z_f]$ when the human–robot collaborative motion stops. Through the analysis of HMFR data, it is found that the motion data are unstable and not suitable for the training of the model when the motion velocity is less than 0.001 m/s. Therefore, the motion data when the motion velocity is greater than 0.001 m/s are selected as the first frame data of the training set, and 50 frames of data for each sample are selected as the training data [30]. The training data input set is

$$\begin{aligned}\boldsymbol{X} = [&\boldsymbol{X}_{r1}^{(i)}, \ldots, \boldsymbol{X}_{rd}^{(i)}, \dot{\boldsymbol{X}}_{r1}^{(i)}, \ldots, \dot{\boldsymbol{X}}_{rd}^{(i)}, \ddot{\boldsymbol{X}}_{r1}^{(i)}, \ldots \\ &\ddot{\boldsymbol{X}}_{rd}^{(i)}, \boldsymbol{F}_{r1}^{(i)}, \ldots, \boldsymbol{F}_{rd}^{(i)}]_{i=1}^{N_t}\end{aligned} \tag{4}$$

where the superscript (i) represents the sample index, $d = 50$, and $N_t = 360$ is the number of samples.

The training data output set is

$$\mathbf{Y}_f = \left[x_f^{(i)}, y_f^{(i)}, z_f^{(i)}\right]_{i=1}^{N_t}. \tag{5}$$

The optimized hyperparameters can be obtained by substituting the training dataset into (2).

The information in the new input data $\boldsymbol{X}_*$ is the same as that in the training data. The difference is that $\boldsymbol{X}_*$ is the human–robot collaborative motion data from moment t-d to moment t. That is

$$\begin{aligned}\boldsymbol{X}_* = \Big[&\boldsymbol{X}_{r(t-d)}^{(i)}, \ldots, \boldsymbol{X}_{rt}^{(i)}, \dot{\boldsymbol{X}}_{r(t-d)}^{(i)}, \ldots, \dot{\boldsymbol{X}}_{rt}^{(i)} \\ &\ddot{\boldsymbol{X}}_{r(t-d)}^{(i)}, \ldots, \ddot{\boldsymbol{X}}_{rt}^{(i)}, \boldsymbol{F}_{r(t-d)}^{(i)}, \ldots, \boldsymbol{F}_{rt}^{(i)}\Big]_{i=1}^{N_t}\end{aligned}, t > d \tag{6}$$

Thus, $\boldsymbol{X}_*$ is changing dynamically. When given a new input $\boldsymbol{X}_*$, the predicted output values $f(\boldsymbol{X}_*)$ and Y obey a joint distribution

$$\begin{bmatrix} Y \\ f(\boldsymbol{X}_*) \end{bmatrix} \sim N\left(\begin{pmatrix} u(\boldsymbol{X}) \\ u(\boldsymbol{X}_*) \end{pmatrix}, \begin{bmatrix} \tilde{\boldsymbol{K}} & \boldsymbol{K}(\boldsymbol{X}, \boldsymbol{X}_*) \\ \boldsymbol{K}(\boldsymbol{X}_*, \boldsymbol{X}) & \boldsymbol{K}(\boldsymbol{X}_*, \boldsymbol{X}_*) \end{bmatrix}\right) \tag{7}$$

where $\boldsymbol{K}(\boldsymbol{X}, \boldsymbol{X}_*)$ is the covariance matrix between the training set and the new input data and $\boldsymbol{K}(\boldsymbol{X}, \boldsymbol{X}_*) = \boldsymbol{K}(\boldsymbol{X}_*, \boldsymbol{X})^T$, $\tilde{\boldsymbol{K}} = \boldsymbol{K}(\boldsymbol{X}, \boldsymbol{X}) + \sigma_n^2 \boldsymbol{I}_n$.

According to (7), the distribution of the predicted output value $f(\boldsymbol{X}_*)$ can be written as

$$f(\boldsymbol{X}_*)|\boldsymbol{X}, y, \boldsymbol{X}_* \sim N(\bar{f}(\boldsymbol{X}_*), \mathrm{cov}(f(\boldsymbol{X}_*))) \tag{8}$$

where $\bar{f}(\boldsymbol{X}_*) = \boldsymbol{K}(\boldsymbol{X}, \boldsymbol{X}_*)\tilde{\boldsymbol{K}}^{-1}Y$, $\mathrm{cov}(f(\boldsymbol{X}_*)) = \boldsymbol{K}(\boldsymbol{X}_*, \boldsymbol{X}_*) - \boldsymbol{K}(\boldsymbol{X}_*, \boldsymbol{X})\tilde{\boldsymbol{K}}^{-1}\boldsymbol{K}(\boldsymbol{X}, \boldsymbol{X}_*)$.

From (8), the output value follows the Gaussian distribution whose mean value is $\bar{f}(\boldsymbol{X}_*)$ and covariance is $\mathrm{cov}(f(\boldsymbol{X}_*))$; then, its probability density function is

$$p(\boldsymbol{X}_t) = N(\boldsymbol{X}_t|\bar{f}(\boldsymbol{X}_*), \mathrm{cov}(f(\boldsymbol{X}_*))) \tag{9}$$

where $\boldsymbol{X}_t = [x_t, y_t, z_t]$ is the target position set in Fig. 3.

In Section III-A, a total of six targets are set. Six target positions are substituted into (9) to obtain the probability that the target predicted by the input data $\boldsymbol{X}_*$ belongs to each preset target. The preset target corresponding to the maximum probability is the target that the human intends to reach.

IV. Role Dynamic Assignment Module

A. Role Dynamic Assignment Strategy

Fig. 4 shows the RDA strategy diagram. The strategy mainly consists of a RDA fuzzy controller and a quantization factor selection fuzzy controller. $k_1 \sim k_5$ is the quantization factor.

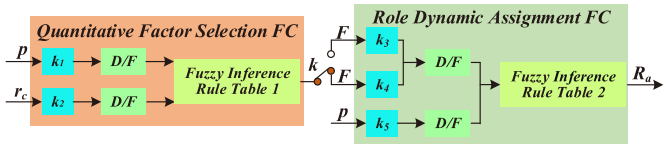

Fig. 4. Role dynamic assignment strategy diagram of the robot.

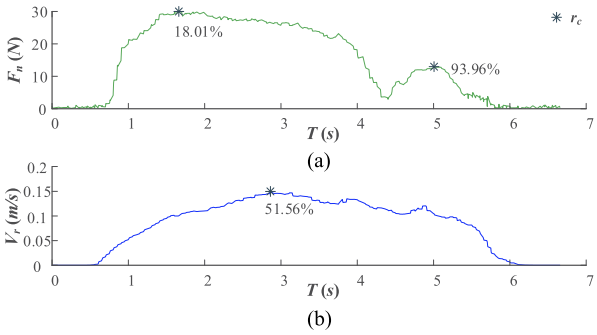

Fig. 5. Interactive force curve (a) and velocity curve (b) of the robot end-effector.

They are set for the scale transformation of the clear value (input), and their function is to make the variable expand or shrink in a certain proportion to match well with the fuzzification module D/F. The fuzzification module D/F uses the membership function to map the input processed by quantized factors to a fuzzy subset in the fuzzy domain (the input fuzzification). The fuzzification input obtains the fuzzification output by fuzzy logic inference.

The input of the quantization factor selection fuzzy controller is the target prediction probability p and r_c. r_c is the ratio of the displacement corresponding to the robot position at time t to the total displacement, that is, $r_c = \|\boldsymbol{X}_r(t) - \boldsymbol{X}_0\|/\|\boldsymbol{X}_f - \boldsymbol{X}_0\|$. $\mathbf{X}_r(t)$ is the position of the robot's end at time t, and $\mathbf{X}_0$ and $\mathbf{X}_f$ are the positions of the starting point and the target point, respectively. The output is the selected quantization factor k, namely, k_3 or k_4. The input of the RDA fuzzy controller is p, F_n, and k. The output is the role the robot will play at the next moment, namely, "leader," "follower," or "uncertain."

B. HMFR Experimental Data Analysis

To provide a basis for the design of membership functions and fuzzy inference rules of the fuzzy controller, the trajectory and interaction force of HMFR were analyzed. Meanwhile the velocity curve (V_r) and interaction force curve (F_n) of the robot were obtained, as shown in Fig. 5. F_n and V_r are all L2 norms of Cartesian spaces.

Through the analysis of HMFR experimental data, it is found that the interactive force curve sometimes has two peaks, as shown in Fig. 5(a). The interaction force curve's first force peak (F_{n1}) appears at 1.6 s ($r_c = 18.01\%$). The robot is at the beginning of its motion. Thus, the first force peak is the maximum force exerted by the participant to guide the robot. The interaction force curve's second force peak (F_{n2}) appears at 5.0 s ($r_c = 93.96\%$). The robot is at the end of motion. Therefore, the second force peak of the interaction force curve is the maximum external force exerted by the participant to make the robot stop near the target point. From Fig. 5(b), the HMFR velocity curve presents a clear "bell shape," which is consistent with the characteristics of the jerk model. The peak value of the velocity curve appears at 2.8 s, and the corresponding r_c value is 51.56%.

TABLE I
INTERACTIVE FORCE PEAK AND VELOCITY PEAK, AS WELL AS THE MEAN AND STANDARD DEVIATION OF r_c

	Peak (N)		*r_c (%)*	
	Mean	*Std*	*Mean*	*Std*
F_{n1}	33.0274	6.8186	22.04	9.84
F_{n2}	9.8454	5.7311	88.33	9.29
V_r	-	-	56.38	8.17

The peaks of interaction force and velocity and their corresponding r_c values were statistically analyzed for all HMFR, and the results are shown in Table I. Table I shows that the mean values of F_{n1} and F_{n2} are 33.0274 and 9.8454 N, respectively. Because participants only need to adjust the robot position in a small range near the target point, the value of F_{n2} is generally smaller than F_{n1}. The mean r_c values of F_{n1}, F_{n2}, and peak velocity are 22.04%, 88.33%, and 56.38%, respectively.

C. Fuzzy Controller

From the analysis of the interaction force of HMFR, it can be seen that the participant strongly intends to play the "leader" role in the two places. One is that at the beginning of the HMFR, the participants exert a large force to guide the robot motion. The other is that in the stopping phase of motion, the participant exerts a large external force to adjust the stopping position of the robot. However, the interaction force that the participant expresses the intention to play the "leader" role is different (the physical domain of the interaction force is different). The mean value of the interaction force when the participants expressed their intention to play the "leader" role in the beginning phase of the motion was much higher than that in the stop phase, as shown in Table I. The membership functions and the fuzzy inference rules are the same in the two places. Therefore, the different quantization factors can be set to scale the input to ensure that the physical domain of the input is the same as the fuzzy domain.

In the robot motion beginning phase, the mean and the standard deviation of the interaction force in which the participant strongly expresses the intention of playing the "leader" role are 33.0274 and 6.8186 N, respectively. The physical and fuzzy domains of the input of the fuzzy controller can be set as [0, 40] (N), and the quantization factor $k_3 = 1$. In the robot motion stop phase, the mean and the standard deviation of the interaction force in which the participant strongly expresses the intention of playing the "leader" role are 9.8454 and 5.7311 N, respectively. The physical domain in which the fuzzy controller input can be set as [0, 15] (N). Because the fuzzy domain of the input is [0, 40] (N), the quantization factor $k_4 = 2.67$.

TABLE II
FUZZY INFERENCE RULES FOR ROLE DYNAMIC ASSIGNMENT

	R_a	p AVL	AL	AM	AH	AVH
F_n	FVS	RF	RF	ID	RL	RL
	FS	RF	RF	ID	RL	RL
	FM	RF	RF	RL	RL	RL
	FL	RF	RF	RF	RF	RL
	FVL	RF	RF	RF	RF	RF

TABLE III
FUZZY INFERENCE RULES FOR QUANTIZATION FACTOR SELECTION

	k	p AVL	AL	AM	AH	AVH
r_c	PB	k_3	k_3	k_3	k_3	k_3
	PM 1	k_3	k_3	k_3	k_3	k_3
	PM 2	k_3	k_3	k_3	k_3	k_3
	PS	k_3	k_4	k_4	k_4	k_4

The RDA fuzzy controller input F_n selects five fuzzy subsets: very small interaction force (FVS), small interaction force (FS), medium interaction force (FM), large interaction force (FL), and very large interaction force (FVL). These five fuzzy subsets are used for the fuzzy domain [0, 40] (N) covering F_n. According to the mean and the standard deviation of the two peaks of HMFR interaction force F_n, the membership functions of the five fuzzy subsets are designed as follows:

$$FVS = 1/(1+\exp(0.9(F_n-7))), 0 \le F_n \le 15 \quad (10)$$

$$FS = \exp(-(F_n-12)^2/18), 0 \le F_n \le 25 \quad (11)$$

$$FM = \exp(-(F_n-20)^2/18), 10 \le F_n \le 30 \quad (12)$$

$$FL = \exp(-(F_n-28)^2/18), 15 \le F_n \le 40 \quad (13)$$

$$FVL = 1/(1+\exp(-0.9(F_n-34))), 25 \le F_n \le 40. \quad (14)$$

The RDA fuzzy controller input p selects five fuzzy subsets: very low accuracy (AVL), low accuracy (AL), medium accuracy (AM), high accuracy (AH), and high accuracy (AVH). The five fuzzy subsets cover the fuzzy domain [0, 100] (%) of robot target prediction probability p. The membership functions of the five fuzzy subsets are as follows:

$$AVL = 1/(1+\exp(0.6(p-18))), 0 \le p \le 30 \quad (15)$$

$$AL(= \exp(-(p-30)^2/162), 0 \le p \le 60 \quad (16)$$

$$AM = \exp(-(p-50)^2/162), 20 \le p \le 80 \quad (17)$$

$$AH = \exp(-(p-70)^2/162), 40 \le p \le 100 \quad (18)$$

$$AVH = 1/(1+\exp(-0.4(p-80))), 60 \le p \le 100. \quad (19)$$

The physical and fuzzy domains of the prediction probability p of the target are the same. Therefore, $k_1 = k_5 = 1$.

The final result of the RDA fuzzy controller output R_a is robot leader (RL), robot follower (RF), or indeterminate (ID). The fuzzy inference rule is designed according to the experience of the human experts, as shown in Table II. When R_a is "ID," the robot maintains the role played at the last moment.

Both input variables of the RDA fuzzy controller are divided into five fuzzy subsets. Therefore, there are 25 fuzzy inference rules in total. The RDA fuzzy inference rule table can be understood as follows: "IF ($\mathbf{p}$ is **AVL**) AND ($\boldsymbol{F}_n$ is **FVS**) THEN $\boldsymbol{R}_a$ is **RF**." The input p increases from left to right. F_n increases from top to bottom. The output R_a gradually changes from "RF" to "RL" from top left to bottom right.

The quantization factors of the RDA fuzzy controller input interaction force F_n are k_3 and k_4. Therefore, this study designed a quantization factor selection fuzzy controller to select quantization factors according to target prediction probability and current motion phase.

According to HMFR data analysis, the mean values of r_c corresponding to interaction force peak 1 (F_{n1}), interaction force peak 2 (F_{n2}), and peak velocity are 22.04%, 88.33%, and 56.38%, respectively, as shown in Table I.

Based on these three nodes, human–robot collaborative motion can be roughly divided into four phases: the beginning phase (PB), middle phase 1 (PM 1), middle phase 2 (PM 2), and the stop phase (PS). Therefore, four fuzzy subsets, namely, PB, PM 1, PM 2, and PS, are selected to cover the fuzzy domain [0, 100] (%) of input r_c

$$PB = 1/(1+\exp(0.2(r_c-20))), 0 \le r_c \le 50 \quad (20)$$

$$PM1 = \exp(-(r_c-38)^2/200), 0 \le r_c \le 70 \quad (21)$$

$$PM2 = \exp(-(r_c-70)^2/200), 30 \le r_c \le 100 \quad (22)$$

$$PS = 1/(1+\exp(-0.3(r_c-80))), 60 \le r_c \le 100. \quad (23)$$

Because the physical domain of r_c is the same as the fuzzy domain, $k_2 = 1$.

The quantization factor selection fuzzy controller output is k_3 or k_4. The fuzzy inference rules of the quantitative factors designed according to the participants' experience are shown in Table III.

p and r_c are divided into 5 and 4 fuzzy sets, respectively. Therefore, there are 20 fuzzy inference rules in total. The quantization factor selection fuzzy inference rule table can be understood as follows: "IF ($\mathbf{p}$ is **AVL**) AND ($\mathbf{r}_c$ is **PB**) THEN $\mathbf{k}$ is $\mathbf{k}_3$." The input p increases from left to right. r_c increases from top to bottom. The output k gradually changes from "k_3" to "k_4" from top left to bottom right.

V. ROBOT MOTION PLANNING MODULE

In this section, the robot motion planning module is established for the problem of robot motion planning in human–robot collaborative motion. Since the robot will play different roles in human–robot collaborative motion, the robot motion planning module is divided into an admittance control-based motion planning submodule and a humanlike motion planning submodule. These two submodules are used for robot motion planning when the robot plays the "follower" and "leader" roles, respectively.

a) Admittance control-based motion planning submodule: When the robot plays the "follower" role, the admittance controller can be designed to control the motion of the robot to obey the human [22], [26]. The robot Cartesian space admittance control model is [31], [32]

$$\boldsymbol{M}(\ddot{\boldsymbol{X}}_d - \ddot{\boldsymbol{X}}_r) + \boldsymbol{C}(\dot{\boldsymbol{X}}_d - \dot{\boldsymbol{X}}_r) + \boldsymbol{K}(\boldsymbol{X}_d - \boldsymbol{X}_r) = \boldsymbol{F} \tag{24}$$

where $\boldsymbol{M} \in R^{3\times3}$, $\boldsymbol{C} \in R^{3\times3}$, and $\boldsymbol{K} \in R^{3\times3}$ are the virtual mass matrix, virtual damping matrix, and virtual stiffness matrix, respectively; $\boldsymbol{F} = [f_x, f_y, f_z]^T$ is the cartesian space interaction force vector; $\boldsymbol{X}_d = [x_d, y_d, z_d]^T$ is the desired position vector.

For convenient applications in the control of industrial robots, (24) can be converted to its discrete format to solve the desired trajectory of the robot [33]

$$\ddot{\boldsymbol{X}}_d(t+1) = \boldsymbol{M}^{-1}(\boldsymbol{F} - \boldsymbol{C}\dot{\tilde{\boldsymbol{X}}} - \boldsymbol{K}\tilde{\boldsymbol{X}}) + \ddot{\boldsymbol{X}}_r(t) \tag{25}$$

$$\dot{\boldsymbol{X}}_d(t+1) = \dot{\boldsymbol{X}}_r(t) + T\ddot{\boldsymbol{X}}_d(t+1) \tag{26}$$

$$\boldsymbol{X}_d(t+1) = \boldsymbol{X}_r(t) + T\dot{\boldsymbol{X}}_d(t+1) \tag{27}$$

where $\boldsymbol{X}_d(t+1)$, $\dot{\boldsymbol{X}}_d(t+1)$, and $\ddot{\boldsymbol{X}}_d(t+1)$ are the desired position, desired velocity, and desired acceleration at moment $t+1$, respectively; $\tilde{\boldsymbol{X}} = \boldsymbol{X}_r(t) - \boldsymbol{X}_r(t-1)$; T is the system communication cycle between the robot controller and the servo driver.

When the robot plays the "follower" role, the admittance control-based motion planning submodule obtains the desired position, desired velocity, and desired acceleration of the robot at the next moment from (25) to (27) according to the robot's current position, current velocity, current acceleration, and interaction force. Finally, the desired position, desired velocity, and desired acceleration of the robot are passed to the robot controller to control the robot to follow the desired trajectory.

b) Humanlike motion planning submodule: When the robot plays the "leader" role, to make the robot's motion conform to the human's subjective cognition and to improve the satisfaction of HMRDA and the stability of the robot's motion, humanlike motion planning was performed for the robot. According to the data analysis of HMFR, the velocity curve of HMFR presents a "bell shape." Therefore, the jerk model is adopted to represent the velocity of HMRDA [34]

$$\dot{\boldsymbol{X}}_r(t) = (\boldsymbol{X}_0 - \boldsymbol{X}_f)\left(60\tau^3 - 30\tau^4 - 30\tau^2\right)/t_f \tag{28}$$

where $\dot{\boldsymbol{X}}_r(t)$ is the robot end-effector's velocity at time t; Moreover, $\tau = t/t_f$, and t_f is the duration of HMRDA.

The total duration t_f of HMRDA can be determined by Fitz's law [34]

$$t_f = a + b\log_2(2^{\sim}A/W) \tag{29}$$

where A is the Euclidean distance between $\boldsymbol{X}_0$ and $\boldsymbol{X}_f$, and W is the size of the target; Based on the experimental device in Fig. 3, W is set to 20 mm; a and b are undetermined coefficients, according to the experimental data of Section III-A, the values of a and b are obtained by the regression method, they are $a = 14.2577$ and $b = 1.9468$, respectively.

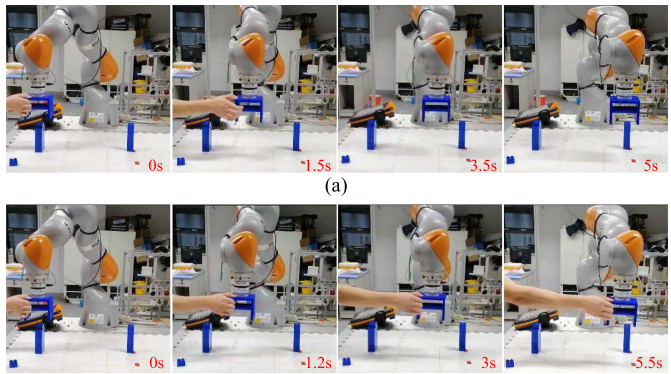

Fig. 6. Human–robot collaborative motion process. HMRDA process is shown in (a). HMFR process is shown in (b).

To determine the τ value in the jerk model when the robot changes from the "follower" role to the "leader" role, (28) is integrated, and the results are as follows:

$$\boldsymbol{X}_r(t) = \boldsymbol{X}_0 + (\boldsymbol{X}_0 - \boldsymbol{X}_f)\left(15\tau^4 - 6\tau^5 - 10\tau^3\right). \tag{30}$$

By substituting the current position $\boldsymbol{X}_r(t)$ of the robot into (30), the value of τ at the current moment t can be obtained. When $0 \le \tau \le 1$, (30) is monotonically increasing; thus, there is a unique τ for any given $\boldsymbol{X}_r(t)$ that makes (30) true. By substituting the τ value at the next moment into (28) and (30), the desired velocity $\dot{\boldsymbol{X}}_d(t+1)$ and desired position $\boldsymbol{X}_d(t+1)$ at the next moment can be obtained. The desired acceleration $\ddot{\boldsymbol{X}}_d(t+1)$ is obtained by differentiating the velocity.

VI. HMRDA Experiment

A. Experimental Setup and Experimental Design

To verify the performance of HMRDA and the effectiveness of the RDA method, a HMRDA experiment was performed. Since the existing role assignment method and the role assignment method in this article solve different problems, the role assignment method in this article cannot be compared with the existing role assignment method. However, we designed HMFR experiments and compared the results of HMFR experiments with those of HMRDA experiments to show the advantages of the proposed role assignment method.

The experimental scene, settings of the starting point and the target point, and participants of HMRDA experiment are the same as those of HMFR, as shown in Fig. 3. The difference is that in the HMRDA experiment, the robot's role can change between the "leader" role and the "follower" role. In the HMRDA experiment, because the robot did not know the target point that the participant intended to go to at the beginning, the participant first guided the robot to move through interactive force, and the robot was in a state of obedience to the participant's motion. At this time, the human–robot collaborative motion process is 0 to 1.5 s of Fig. 6(a). The RDA module assigns the role of the robot according to the target prediction probability and the robot motion data. When the robot was assigned the "follower" role, the robot continued to follow the participant's

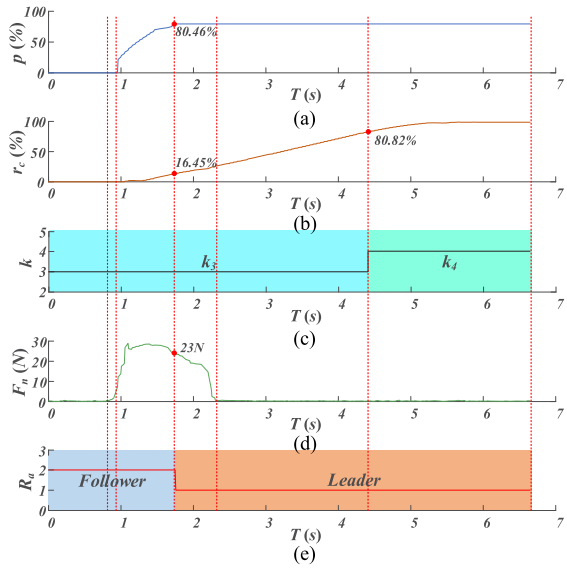

Fig. 7. Input and output changes of HMRDA. p change curve is shown in (a). r_c change curve is shown in (b). The change of quantization factor k is shown in (c), where "3" presents for "k_3" and "4" presents for "k_4." F_n change curve is shown in (d). R_a change curve is shown in (e), where "1" means the robot plays the "leader" role, and "2" means the robot plays the "follower" role.

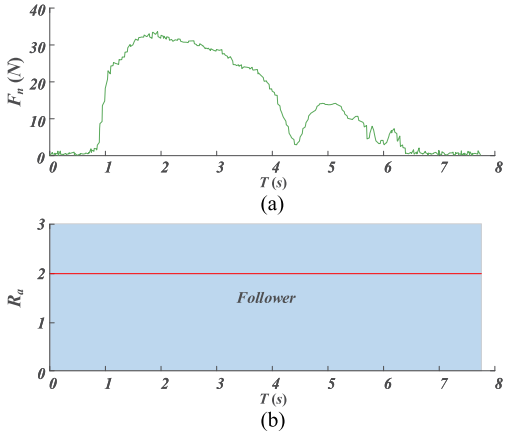

Fig. 8. Input and output changes of HMFR. F_n change curve is shown in (a). R_a change curve is shown in (b).

motions. When the robot was assigned the "leader" role, the robot planned its own motion online according to the prediction of the participant's intention and guided the participant to the predicted target position. When participants felt that the robot predicted their own motion intentions correctly, they actively followed the robot's motions or withdrew from the collaborative motion. At this time, the human–robot collaborative motion process is 1.5–5 s of Fig. 6(a). When the participant was not satisfied with the current motion of the robot, the participant could exert active force again and become the "leader." Through real-time feedback of motion data, the role and motion of the robot can be adjusted in real time. However, in the HMFR experiment, the participants always guided the robot's motion through the interaction force, as shown in Fig. 6(b).

B. Experimental Results and Performance Assessment

To illustrate the robot role change process, the input and output of HMRDA and HMFR are shown, respectively, as shown in Figs. 7 and 8. From Fig. 7, the interaction force gradually increases from 0.8 s, while the other inputs and outputs remain basically unchanged. The p and r_c values also gradually increase from 0.95 s. The input data of the target prediction module are the motion data from moment *t-d* to moment *t*. That is, the input changes dynamically. Therefore, p is constantly changing between 0.95 and 1.8 s. Because p is low at this time, the target that the participant intends to go to cannot be determined; thus, the role assigned by the RDA module to the robot is the follower. At approximately 1.8 s, p reaches 80.46%, the corresponding fuzzy set is AVH, r_c is 16.45%, and the corresponding fuzzy set is PB. The quantization factor selected by the fuzzy inference rule (see Table III) is k_3. At this time, the interaction force is 23 N, and the corresponding fuzzy set is FL. According to the fuzzy inference rule (Table II), the robot plays the "leader" role. After the robot plays the "leader" role in HMRDA, the target prediction module no longer performes target prediction. Therefore, p no longer changes after 1.8 s. The robot plans its own motion trajectory according to the current motion information. The participant felt that the robot began to move toward the target they intended to reach and gradually gave up the dominance of the collaborative motion and began to follow the robot or withdraw from HMRDA. Therefore, F_n gradually decreased. At 2.3 s, F_n is close to zero, indicating that the participant no longer controls the robot, the participant is in a fully following state, and the robot fully controls the progress of HMRDA. At 4.3 s, p is 80.46%, the corresponding fuzzy set is AVH, r_c is 80.82%, and the corresponding fuzzy set is PS. The quantization factor selected by the fuzzy inference rule (see Table III) is k_4. At 6.7 s, the robot reaches the target point, and the HMRDA ends. When the robot plays the "leader" role, if the participant feels that the robot's target prediction is wrong or there is a problem in motion planning, the participant can regain dominance by applying external forces.

From Fig. 8, the interaction force F_n is constantly changing, while the value of R_a remains unchanged, which indicates that in HMFR, the human has always played the "leader" role. The human has always been required to guide the robot's motion through the interaction force. The comparison between Figs. 7(d) and 8(a) shows that in HMRDA, humans do not always participate in human–robot collaboration, which is conducive to reducing human workload.

To verify the effectiveness of RDA method, the number of experiments in which the robot played the "leader" role and the duration of each time the robot played the "leader" role in HMRDA were statistically analyzed. The ratio of the number of robots playing the "leader" role to the total number of experiments is 96.91%. The mean duration ratio of the robot playing the "leader" role is 82.00%, and the standard deviation is 4.37%. This indicates that the RDA algorithm based on fuzzy inference can effectively achieve role dynamic assignment and effectively reduce human participation.

TABLE IV
MEAN FRÉCHET DISTANCE, MEAN WORKLOAD, AND F TEST OF THE HUMAN–ROBOT COLLABORATIVE MOTION AT EACH TARGET POINT BASED ON TWO ROLE ASSIGNMENT NETHODS

	k	*1*	*2*	*3*	*4*	*5*	*6*	*Mean*	*F*	*p-value*
$F(X_r, \tilde{X}_r)$	***HMFR*** (m)	0.0865	0.0805	0.0946	0.1088	0.0820	0.0940	0.0911	5.5009	<0.05
	HMRDA (m)	0.0761	0.0734	0.0778	0.0711	0.0635	0.0651	0.0712		
W_h	***HMFR*** $(N{\cdot}m)$	7.7288	13.5953	10.8311	11.6499	12.3365	11.7417	11.3139	15.9552	<0.05
	HMRDA $(N{\cdot}m)$	3.7599	7.2762	6.2451	3.4571	4.0307	2.9043	4.6122		

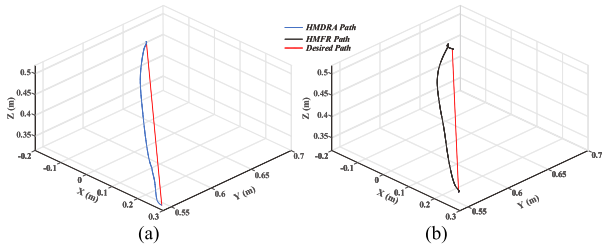

Fig. 9. Human–robot collaborative motion path. HMRDA path is shown in (a). HMFR path is shown in (b).

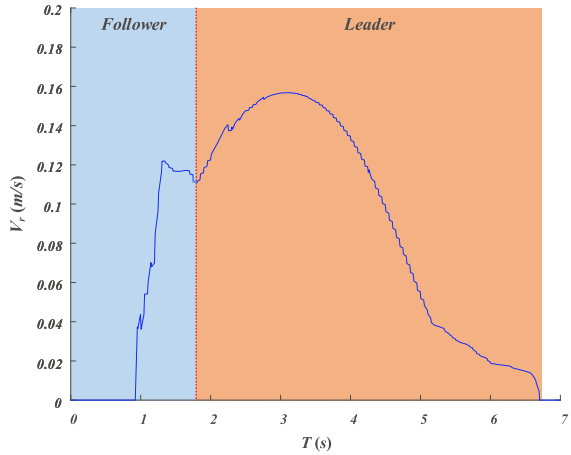

Fig. 10. HMRDA velocity curve.

To more vividly show the influence of the "leader" role of the robot in the human–robot collaborative motion, the 3-D paths of human–robot collaborative motion based on the two role assignment methods are shown respectively. The 3-D path of human–robot collaborative motion is shown in Fig. 9. The solid blue line in Fig. 9(a) is the HMDRA path. The solid black line in Fig. 9(b) is the HMFR path. The red dashed lines in Fig. 9 show the desired path of human–robot collaborative motion. Fig. 9 shows that the HMFR path has a significant fluctuation, showing an irregular curve and a large error with the desired path. Near the target point, a small range of oscillations appears in the human–robot collaborative motion path. The path of HMRDA fluctuated before the robot was assigned the role of "leader." After the robot played the "leader" role, the robot's path was smoother, and the error with the desired path was small.

The investigation of the participants' feelings after the completion of the human–robot collaborative motion found that the participants did not clearly feel when the robot began to become the "leader," but only knew that the robot had become the "leader" when they felt the interaction force became significantly smaller after continuing the motion for a period of time. This occurs because after the robot became the "leader," it performed humanlike motion according to the motion law of the human arm. Thus, the robot's motion velocity had good synchronization with the participants' motion velocity. The velocity curves based on HMRDA are shown in Fig. 10. From Fig. 10, before 1.8 s, the robot plays the "follower" role. At this time, the velocity curve of the robot fluctuates greatly, and the motion stationarity is poor. However, after 1.8 s, the robot plays the "leader" role. At this time, the velocity curve is close to the velocity curve of the jerk model, and the motion stability is good. When the robot transitions roles, the velocity changes smoothly without large fluctuations, indicating that the robot can smoothly realize the role transition. Thus participants have no apparent sense of when the robot becomes the "leader" role.

To quantitatively evaluate the performance differences between HMRDA and HMFR, the path similarity (Fréchet distance) [35] between the actual path and the desired path and the workload [33] of the participant in human–robot collaborative motion were used to conduct a quantitative evaluation of the results under two experimental conditions

$$F(\boldsymbol{X}_r, \tilde{\boldsymbol{X}}_r) = \max_{t\in[0,t_f]} \{d(\boldsymbol{X}_r(t), \tilde{\boldsymbol{X}}_r(t))\} \tag{31}$$

$$W_h = \int_{t_0}^{t_f} \left\| \left| \boldsymbol{F}^T(t) \right| \left| \dot{\boldsymbol{X}}_r(t) \right| \right\| dt \tag{32}$$

where $\boldsymbol{X}_r(t)$ is the actual path from the starting point to the target point; $\tilde{\boldsymbol{X}}_r(t)$ is the desired path from the starting point to the target point; $F(\boldsymbol{X}_r, \tilde{\boldsymbol{X}}_r)$ is the Fréchet distance between the actual path and the desired path; W_h is the human workload in the human–robot collaborative motion.

According to the experimental setting, a total of six participants participated in the HMRDA experiment and HMFA experiment, and each target point performed ten experiments. Equations (31) and (32) were used to calculate the mean Fréchet distance and the participants' mean workload at each target point, respectively, as shown in Table IV.

Table IV shows that there are significant differences in the Fréchet distance ($F(1, 10) = 5.5009 > 4.965$, p-value < 0.05) and workload ($F(1, 10) = 15.9552 > 4.965$, p-value < 0.05) between the human–robot collaborative motions based on the two role assignment methods. The mean value of the Fréchet distance of HMRDA is smaller than that of HMFR, which indicates that the spatial path of HMRDA is closer to the desired spatial path. The mean workload of participants in HMRDA is also lower than that of HMFR, indicating that participants save more energy efficiently in HMRDA.

In conclusion, the RDA algorithm can effectively implement the role dynamic assignment. There is a significant difference in the performance between HMFR and HMRDA. HMRDA is superior to HMFR in the workload and the path similarity between the actual path and the desired path.

VII. Conclusion

In HMRDA, the robot could understand the current motion behavior of humans through HMRDA data and predict the motion target of humans by combining it with the previously learned knowledge (Gaussian process regression model). According to the current motion information and predicted data, the robot adjusted its role by imitating the logical reasoning thinking of the human and planned its motion according to the current role. Finally, the robot analyzed the response of the collaborator (human) to further deepen or adjust its role and motion. To evaluate the effectiveness of the proposed method, a HMRDA experiment was performed. In the HMRDA experiment, the ratio and mean duration ratio of the robot playing the "leader" role were 96.91% and 82.00%, respectively. This indicated that the RDA algorithm based on target prediction and fuzzy inference could effectively realize role dynamic assignment and keep the robot in the "leader" role for a long time, thus reducing the participation of humans. Compared with HMFR, the mean Fréchet distance and mean participant workload of HMRDA were both smaller. This indicated that the spatial path of HMRDA was closer to the desired path, and participants consumed less energy. Meanwhile, the velocity curve of HMRDA changed smoothly, indicating that the HMRDA framework could ensure the stationarity of motion during role transition. Finally, it achieved the goal of reducing human mental workload and fatigue and gave full play to the advantages of humans and robots. In future work, to further play the advantages of the role dynamic assignment algorithm proposed in this article, we will improve the target prediction algorithm so that the robot can also achieve target prediction when the motion target point is arbitrarily changed in human motion. Meanwhile, the generality of this article's role dynamic assignment algorithm will be improved to extend it to more practical applications.

References

[1] J. Luo, D. Huang, Y. Li, and C. Yang, "Trajectory online adaption based on human motion prediction for teleoperation," *IEEE Trans. Automat. Sci. Eng.*, vol. 19, no. 4, pp. 3184–3191, Oct. 2022.

[2] C. Y. Weng, Q. Yuan, F. Suarez-Ruiz, and I. M. Chen, "A telemanipulation-based human–robot collaboration method to teach aerospace masking skills," *IEEE Trans. Ind. Inform.*, vol. 16, no. 5, pp. 3076–3084, May 2020.

[3] M. Cramer, K. Kellens, and E. Demeester, "Probabilistic decision model for adaptive task planning in human-robot collaborative assembly based on designer and operator intents," *IEEE Robot. Autom. Lett.*, vol. 6, no. 4, pp. 7325–7332, Oct. 2021.

[4] C. Liu and M. Tomizuka, "Modeling and controller design of cooperative robots in workspace sharing human–robot assembly teams," in *Proc. IEEE/RSJ Int. Conf. Intell. Robots Syst.*, 2014, pp. 1386–1391.

[5] A. Sidiropoulos, Y. Karayiannidis, and Z. Doulgeri, "Human–robot collaborative object transfer using human motion prediction based on cartesian pose dynamic movement primitives," in *Proc. IEEE Int. Conf. Robot. Autom.*, 2021, pp. 3758–3764.

[6] J. Zhao, C. Wang, and B. Xie, "Human-like motion planning of robotic arms based on human arm motion patterns," *Robotica*, vol. 41, no. 1, pp. 259–276, Jan. 2023.

[7] Y. He, B. Zhao, X. Qi, S. Li, Y. Yang, and Y. Hu, "Automatic surgical field of view control in robot-assisted nasal surgery," *IEEE Robot. Autom. Lett.*, vol. 6, no. 1, pp. 247–254, Jan. 2021.

[8] M. Deng, Z. Li, K. Yu, C. Chen, and X. Chu, "A learning-based hierarchical control scheme for an exoskeleton robot in human–robot cooperative manipulation," *IEEE Trans. Cybern.*, vol. 50, no. 1, pp. 112–125, Jan. 2020.

[9] A. H. Khan, S. Li, and X. Luo, "Obstacle avoidance and tracking control of redundant robotic manipulator: An RNN-based metaheuristic approach," *IEEE Trans. Ind. Inform.*, vol. 16, no. 7, pp. 4670–4680, Jul. 2020.

[10] Q. Wang, Y. Cheng, W. Jiao, M. T. Johnson, and Y. M. Zhang, "Virtual reality human–robot collaborative welding: A case study of weaving gas tungsten arc welding," *J. Manuf. Process.*, vol. 48, no. 1, pp. 210–217, Jul. 2019.

[11] M. Hagenow, E. Senft, R. Radwin, M. Gleicher, B. Mutlu, and M. Zinn, "Corrective shared autonomy for addressing task variability," *IEEE Robot. Autom. Lett.*, vol. 6, no. 2, pp. 3720–3727, Apr. 2021.

[12] R. J. Ansari and Y. Karayiannidis, "Task-based role adaptation for human-robot cooperative object handling," *IEEE Robot. Autom. Lett.*, vol. 6, no. 2, pp. 3592–3598, Apr. 2021.

[13] L. Peternel, N. Tsagarakis, and A. Ajoudani, "Towards multi-modal intention interfaces for human–robot co-manipulation," in *Proc. IEEE/RSJ Int. Conf. Intell. Robots Syst.*, 2016, pp. 2663–2669.

[14] Z. Al-Saadi, D. Sirintuna, A. Kucukyilmaz, and C. Basdogan, "A novel haptic feature set for the classification of interactive motor behaviors in collaborative object transfer," *IEEE Trans. Haptics*, vol. 14, no. 2, pp. 384–395, Apr.–Jun. 2021.

[15] M. Khoramshahi and A. Billard, "A dynamical system approach for detection and reaction to human guidance in physical human–robot interaction," *Auton. Robots*, vol. 8, no. 44, pp. 1411–1429, Apr. 2020.

[16] E. M. van Zoelen, E. I. Barakova, and M. Rauterberg, "Adaptive leader-follower behavior in human–robot collaboration," in *Proc. IEEE 29th Int. Conf. Robot Hum. Interact. Commun.*, 2020, pp. 1259–1265.

[17] S. Sheikholeslami, A. Moon, and E. A. Croft, "Cooperative gestures for industry: Exploring the efficacy of robot hand configurations in expression of instructional gestures for human IEEE robot interaction," *Int. J. Robot. Res.*, vol. 5, no. 36, pp. 699–720, Apr. 2017.

[18] N. Stefanov, A. Peer, and M. Buss, "Role determination in human-human interaction," in *Proc. World Haptics 3rd Joint EuroHaptics Conf. Symp. Haptic Interfaces Virtual Environ. Teleoperator Syst.*, 2009, pp. 51–56.

[19] C. M. T. Samuel and K. P. Tee, "Unified human IEEE robot shared control with application to haptic telemanipulation," in *Proc. IEEE/RSJ Int. Conf. Intell. Robots Syst.*, 2019, pp. 2221–2226.

[20] S. O. Oguz, A. Kucukyilmaz, T. M. Sezgin, and C. Basdogan, "Haptic negotiation and role exchange for collaboration in virtual environments," in *Proc. IEEE Haptics Symp.*, 2010, pp. 371–378.

[21] A. Moertl, M. Lawitzky, A. Kucukyilmaz, M. Sezgin, C. Basdogan, and S. Hirche, "The role of roles: Physical cooperation between humans and robots," *Int. J. Robot. Res.*, vol. 31, no. 13, pp. 1656–1674, 2012.

[22] Y. Li, K. P. Tee, W. L. Chan, R. Yan, Y. Chua, and D. K. Limbu, "Continuous role adaptation for human IEEE robot shared control," *IEEE Trans. Robot.*, vol. 31, no. 3, pp. 672–681, Jun. 2015.

[23] R. K. Leskovar, J. Čamernik, and T. Petrič, "Leader IEEE follower role allocation for physical collaboration in human dyads," *Appl. Sci.*, vol. 11, no. 19, pp. 1–23, Sep. 2021.

[24] P. Evrard and A. Kheddar, "Homotopy-based controller for physical human IEEE robot interaction," in *Proc. 18th RO-MAN IEEE Int. Symp. Robot Hum. Interactive Commun.*, 2009, pp. 1–6.

[25] P. Evrard and A. Kheddar, "Homotopy switching model for dyad haptic interaction in physical collaborative tasks," in *Proc. World Haptics Third Joint EuroHaptics Conf. Symp. Haptic Interfaces Virtual Environ. Teleoperator Syst.*, 2009, pp. 45–50.

[26] Y. Li, K. P. Tee, R. Yan, W. L. Chan, and Y. Wu, "A framework of human–robot coordination based on game theory and policy iteration," *IEEE Trans. Robot.*, vol. 32, no. 6, pp. 1408–1418, Dec. 2016.

[27] A. Takagi, Y. Li, and E. Burdet, "Flexible assimilation of Human's target for versatile human IEEE robot physical interaction," *IEEE Trans. Haptics*, vol. 14, no. 2, pp. 421–431, Apr.–Jun. 2021.

[28] D. Sirintuna, I. Ozdamar, Y. Aydin, and C. Basdogan, "Detecting human motion intention during pHRI using artificial neural networks trained by EMG signals," in *Proc. IEEE 29th Int. Conf. Robot Hum. Interact. Commun.*, 2020, pp. 1280–1287.

[29] J. W. Nevin, F. J. Vaquero-Caballero, D. J. Ives, and S. J. Savory, "Physics-informed Gaussian process regression for optical fiber communication systems," *J. Lightw. Technol.*, vol. 39, no. 21, pp. 6833–6844, Nov. 2021.
[30] J. Zhao, S. Gong, and B. Xie, "Human arm motion prediction in human–robot interaction based on a modified minimum jerk model," *Adv. Robot.*, vol. 35, no. 3, pp. 205–218, Nov. 2021.
[31] G. Kang, H. S. Oh, J. K. Seo, U. Kim, and H. R. Choi, "Variable admittance control of robot manipulators based on human intention," *IEEE/ASME Trans. Mechatron.*, vol. 24, no. 3, pp. 1023–1032, Jun. 2019.
[32] L. Zlajpah and T. Petric, "Unified virtual guides framework for path tracking tasks," *Robotica*, vol. 38, no. 10, pp. 1807–1823, Oct. 2020.
[33] J. Duan, Y. Gan, M. Chen, and X. Dai, "Adaptive variable impedance control for dynamic contact force tracking in uncertain environment," *Robot. Auton. Syst.*, vol. 32, no. 102, pp. 54–65, Apr. 2018.
[34] S. Gong, J. Zhao, and B. Xie, "Robot motion planning with human-like motion patterns based on human arm movement primitive chains," in *Proc. IEEE Int. Conf. Robot. Autom.*, 2021, pp. 8373–8379.
[35] C. Lyu, X. Wu, Y. Liu, and Z. Liu, "A partial-Fréchet-distance-based framework for bus route identification," *IEEE Trans. Intell. Transp. Syst.*, vol. 23, no. 7, pp. 9275–9280, Jul. 2022.

Chengyun Wang was born in Shandong, China in 1992. He is currently working toward the Ph.D. degree in mechanical engineering with the Beijing University of Technology, Beijing, China.

He has authored nine articles. His research interests include robot humanlike motion planning and human–robot collaboration.

Jing Zhao was born in Beijing, China in 1961. He received the Ph.D. degree in mechanical engineering from the Beijing University of Technology, Beijing, China, in 1998.

From 1998 to 2000, he was an Associate Professor with the Faculty of Materials and Manufacturing, Beijing University of Technology, where he has been a Professor since 2000. He has authored more than 130 articles. His research interests include redundant robot motion planning, human–robot interaction, and robot teleoperation.

Dr. Zhao was a Senior Member of Chinese Mechanical Engineering Society.